

# Simultaneous Independent Measurement of Splat Diameter and Cooling Time during Impact on a Substrate of Plasma-Sprayed Molybdenum Particles

P. Gougeon and C. Moreau

(Submitted 2 February 1998; in revised form 19 October 2000)

In thermal spray processes, the coating structure is the result of flattening and cooling of molten droplets on the substrate. The study of the cooling time and evolution of the splat size during impact is then of the highest importance to understand the influence of the spray parameters and substrate characteristics on the coating structure. Measurement of particle temperature during impact requires the use of a high-speed two-color pyrometer to collect the thermal emission of the particle during flattening. Simultaneous measurement of the splat size with this pyrometer is difficult since the size of the particle can change as it cools down. To measure the splat size independently, a new measurement technique has been developed. In this technique, the splat size is measured from the attenuation of the radiation of a laser beam illuminating the particle during impact. Results are presented for plasma-sprayed molybdenum particles impacting on a glass substrate at room temperature. It is shown that the molybdenum splat reaches its maximum extent about 2  $\mu\text{s}$  after the impact. In this work, we show that this increase of the splat surface is followed by a phase during which the splat size decreases significantly during 2 to 3  $\mu\text{s}$ .

**Keywords** cooling time, flattening, high speed pyrometry, laser, liquid metal, molybdenum, particle impact, plasma spraying

## 1. Introduction

Thermal-sprayed coatings are built from the successive impacts of molten, or partially molten, droplets, which flatten, cool down, and solidify on a substrate, or on previously deposited layers. The way the sprayed droplets impact on a solid surface is of the utmost importance to control the microstructure of the thermal-sprayed coatings, as well as their adhesion and performance. It is clear that the velocity of the sprayed particles before impact and their viscosity are important parameters influencing the formation of the resulting splats on the substrate. This influence was, in particular, studied by Madejski,<sup>[1,2]</sup> who gave expressions of the diameter of the splat as a function of the velocity and viscosity of the sprayed droplet. In the analytical model of Madejski, the substrate is perfectly smooth and the thermal contact is assumed to be perfect. Although these assumptions are not valid in typical thermal spray conditions, the model gives values of splat size, which can often be used as guidelines.

Since Madejski's pioneering work, numerous studies, both theoretical and experimental, have been undertaken on the par-

article/substrate interaction. Some models can deal with the solidification process starting before the particle has finished spreading on the substrate (*e.g.*, Ref 3 to 6). In most recent models, it is possible to take into account the thermal contact resistance at the particle/substrate interface<sup>[7,8]</sup> and a regular surface roughness.<sup>[9]</sup> As the thermal contact resistance is not known *a priori*, it needs to be experimentally determined to apply the model in a given situation. For example, Ref 10 gives values of the thermal contact resistance, which depend on the substrate roughness and oxidation state.

On the experimental side, different studies have shown the influence of the particle state before impact (molten state and velocity)<sup>[11]</sup> and of the substrate roughness on the splat formation.<sup>[12,13]</sup> It is also well known, although more recently quantified,<sup>[14,15]</sup> that the substrate temperature plays an important role on the splat shape, even for smooth substrates. Indeed, there exists a substrate temperature above which the shape of the splat is regular and presents a disklike shape (no splashing). Below this transition temperature, the shape of the splat becomes irregular (finger type), revealing some splashing of material on the substrate. For a given substrate material, Fukomoto *et al.*<sup>[15]</sup> have shown that the value of this transition temperature is strongly dependent on the nature of the sprayed material. In another paper, Huang *et al.*<sup>[16]</sup> have also shown that the nature of the substrate has some influence on the substrate transition temperature. In this latter work, both the substrate thermal conductivity and wettability are proposed to be the main characteristics controlling the regularity of the splat shape. This explanation is different, but not in contradiction, to the one discussed in Ref 7, which emphasizes the importance of the thermal contact at the interface between the particle and the substrate. According to Ref 7, pre-

**P. Gougeon**, formerly with National Research Council Canada, Industrial Materials Institute, Boucherville, PQ, Canada J4B 6Y4, is now with LERMPS, University de Technologie de Belfort-Montbeliard, 90010 Belfort, Cedex, France; and **C. Moreau**, National Research Council Canada, Industrial Materials Institute, Boucherville, PQ, Canada J4B 6Y4. Contact e-mail: patrick.gougeon@utbm.fr.

heating the substrate allows the material to stay above the hypercooling temperature during flattening of the particle (1 to 2  $\mu$ s). When the flattening is completed, the material cools down and solidifies rapidly as a regular splat disk. Without preheating of the substrate, the material in contact with the substrate during the impact cools down below the hypercooling temperature. Consequently, this solid phase disturbs the spreading of the liquid phase leading to an irregular splat.

Study of the influence of the substrate temperature shows the complexity of the phenomena involved in the particle/substrate interaction in plasma spraying, especially in the first microseconds following the impact. These phenomena can be studied by measuring some particle parameters during impact, such as the flattening degree and cooling rate, by using high speed pyrometers.<sup>[17,18]</sup> However, with these systems, it is generally not possible to measure the size of the particle independently of its temperature, as flattening and cooling can occur simultaneously.<sup>[12]</sup> The difficulties come from the fact that the particle temperature and surface are measured from the same signals (particle thermal emission). In this work, a new optical technique aimed at measuring the surface of a particle during impact independently of its temperature is described. Measurements are carried out on plasma-sprayed molybdenum particles impacting on a smooth glass substrate at room temperature.

## 2. Experimental

### 2.1 Experimental Setup

The experimental setup is similar to the one described in Ref 19, except for the laser beam used to measure the particle surface area during flattening. A schematic of this experimental setup is shown in Fig. 1. The setup is protected from an excess of powders and heat by a V-shape metal shield pierced in its central edge. The sprayed particles pass through the shield and two holes before reaching the glass substrate at 120 mm from the plasma torch exit. The first hole, at 40 mm from the substrate, is 1.5 mm in diameter and limits the particle flux to the second hole to prevent clogging. The second hole, located at 25 mm from the substrate, is 800  $\mu$ m in diameter. The holes are aligned in such a way that only particles having a horizontal trajectory can pass through them.

When a particle reaches the substrate region, its thermal radiation is measured in flight just before impact and upon impact on the substrate. The thermal radiation is collected by an optical sensor head consisting of a custom-made lens focusing the collected radiation with a 0.59 magnification on an optical fiber of 800  $\mu$ m core. The optical lens was primarily designed to minimize the chromatic aberrations in the near infrared range (700 to 1000 nm) while giving a very high spatial resolution for on-axis objects.<sup>[20]</sup> The tip of the optical fiber located inside the sensor head is covered with an optical mask opaque to near infrared radiation except for three slits. These slits allow the detection of the particle thermal radiation at three different positions along the particle trajectory without having to align different pyrometers.<sup>[18]</sup> The field of view defined by these three slits is illustrated in Fig. 2. When a particle crosses the field of view of the first two slits, its temperature, velocity, and size can be determined by detecting the thermal radiation emitted by the particle.<sup>[21]</sup> These

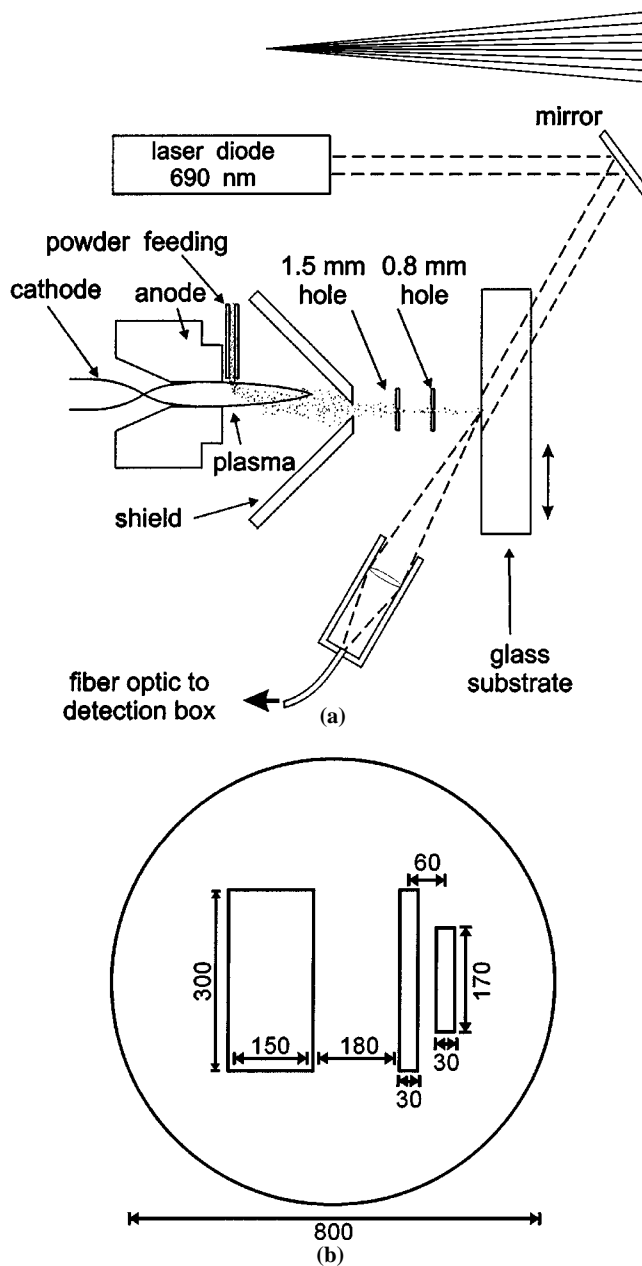


**Fig. 1** (a) Experimental setup and (b) details of the three-slit mask (dimensions in micrometers)

slits define two zones of 50  $\mu$ m width, separated by 100  $\mu$ m (center to center). The third slit is the widest (300  $\times$  150  $\mu$ m) and is used to detect the thermal radiation of the particle upon impact. It defines a square surface of 510  $\mu$ m side on the substrate owing to the 30° angle between the sensor axis and the substrate.

In addition to the detection of the thermal radiation, the third slit on the optical fiber is also used to receive the radiation from a laser diode at 690 nm. This laser diode is located on the back side of the glass substrate and on the axis of the optical sensor head. With this arrangement, in the absence of particles in the observed zone, the totality of the laser radiation included inside the 510  $\mu$ m side square is detected. Inversely, when a splat is present on the glass surface, it blocks a fraction of the laser radiation. The intensity profile of the laser beam used for this measurement is uniform within  $\pm 20\%$  in the 510  $\mu$ m zone. Consequently, assuming that the sprayed material is opaque, the

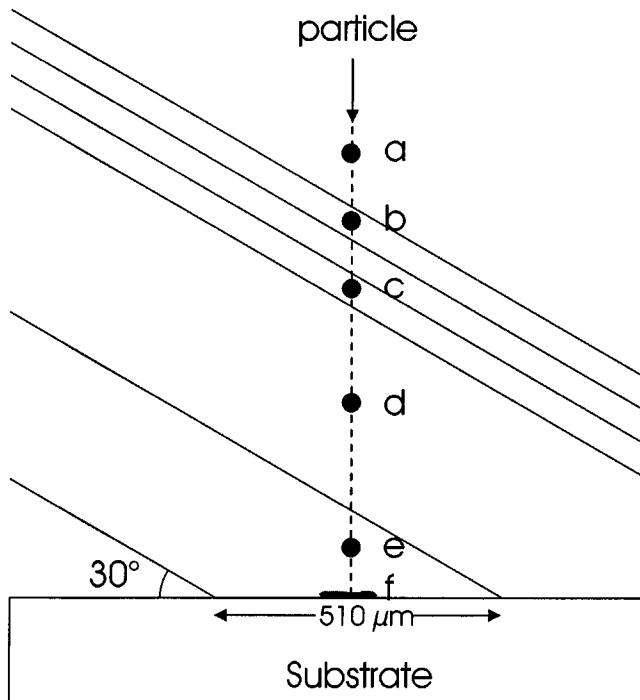


**Fig. 2** Schema of the pyrometer field of view. The particle is seen through the three slits of the optical mask as it moves toward the substrate

attenuation at 690 nm is proportional to the area of the splat surface during the impact.

The radiation (thermal emission and laser radiation) collected through the optical mask is guided by an 8 m long optical fiber toward the detection box containing the optical filters and photodetectors. Following the optical path in this box, the radiation is first separated in two parts with a 50% reflective beam splitter. The reflected part is spectrally filtered at 690 nm ( $\Delta\lambda = 10$  nm) for detection of the laser radiation by an avalanche Si photodetector. On the other side, the transmitted part of the beam is spectrally divided by a dichroic filter and imaged on two avalanche Si photodetectors after transmission through bandpass filters at 790 and 1000 nm. These bandpass filters have been chosen to avoid the main emission lines of argon plasma, which otherwise could bias the measurement of the particle thermal emission.<sup>[22]</sup> The three photodetectors in the detection box have a response time smaller than 0.1  $\mu$ s, which is rapid enough to follow the particle impact signals. The three signals are recorded by a 12-bit (5 MHz bandwidth) digital oscilloscope for off-line analysis.

## 2.2 Signal Analysis

When a particle impacts in the center of the 510  $\mu$ m square, the time evolution of the thermal emission signals at 790 and 1000 nm looks like the one in Fig. 3. The (a) to (f) labels refer to the corresponding positions of the particle in the optics field of view (Fig. 2). At positions (a) and (d), the particle is not seen by detection optics, and then there is no signal on the photodetectors. In positions (b) and (c), the particle is seen twice giv-

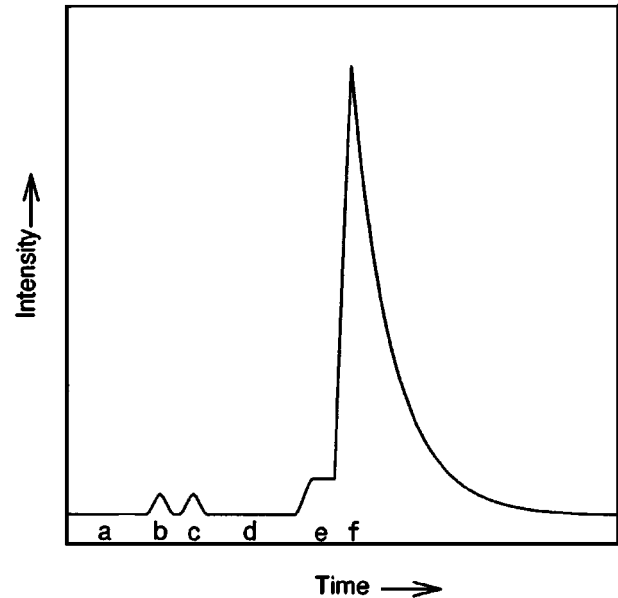


**Fig. 3** Thermal emission signal after collection through a three-slit mask (schematic)

ing rise to a two-peak signal in the photodetectors. The time delay between the two peaks gives the particle velocity, if the optical magnification is known.<sup>[20]</sup> In (e), the in-flight particle is seen by the third slit just before the particle impacts. When the particle impinges on the substrate, it flattens, leading to a rapid increase of the radiating surface and a corresponding signal rise in (f). After having reached a maximum, which depends on the flattening and cooling rates during the particle impact, the thermal emission signal finally decreases during cooling. The temperature of the particle, in-flight and at impact, is obtained by two-color pyrometry from the ratio of the signals collected at 790 and 1000 nm. As the material emissivity is *a priori* unknown, especially at high temperature, the two-color pyrometer is calibrated to measure a gray-body temperature. However, the true temperature and the gray-body temperature can be significantly different for some molten metals, as reported in Ref 19.

As the thermal emission signal is a function of the particle size, particle temperature, and material emissivity, no reliable information on the particle size during impact can be obtained from this signal. A measurement of the particle size, however, is possible by using the signal from the laser diode illuminating the splat from the back side of the glass substrate. Indeed, the attenuation of the laser beam radiation at 690 nm is proportional to the area of the particle surface. A splat equivalent diameter can then be computed as the diameter of the opaque disk blocking the same fraction of laser radiation as the particle during its impact. This computation is based on the assumption that the laser intensity is uniform over the 510  $\mu$ m square defined on the substrate by the third slit on the optical fiber. In practice, a part of the signal detected at 690 nm includes a thermal emission component, which leads to an underestimation of the laser beam attenuation. A simple estimation based on the gray-body assumption shows that, in the present configuration, the splat equivalent diameter can be underestimated by between 8% for a

2000 °C particle and 22% for a 3200 °C particle (extreme case in this study). Although the thermal emission is not negligible, it will be shown later that its influence does not affect the conclusions of this work.

### 2.3 Experimental Procedure

Plasma spraying is carried out with a Plasmadyne SG100 torch (Praxair Surface Technologies, Indianapolis, IN) using the electrodes/gas injector configuration (129-145-130). The plasma torch is operated at 500 A arc current. The gas mixture is 50 L/min Ar with 25 L/min He, which corresponds to 33% of the total volume. The powder is injected internally at a very low feed rate (a few grams/minute) to minimize multiple impacts in the optics field of view at a given time. The sprayed material is dense spherical molybdenum powder, SD152 from Sylvania, (OSRAM SYLVANIA, Chemical & Metallurgical Products, Towanda, PA) sieved to +32 –45  $\mu\text{m}$  to obtain a narrow size range (Ref 13 provides a electron micrograph of the sieved powder).

The experimental setup is aligned according to the sprayed particle trajectory to ensure that most of the particles impacting on the substrate are in the field of view of the third slit. The substrate is made of smooth optical BK7 type glass ( $R_a = 0.02 \mu\text{m}$ ). It can be moved vertically by using a step motor each time an event is recorded. In this way, the probability of having more than one impact in the observed zone is minimized. The position of each splat is noted on the substrate surface in order to examine them under microscope. This procedure allows us to correlate the signals recorded on the oscilloscope to the corresponding impacts on the substrate.

## 3. Results

The thermal emission signals and the signal at 690 nm are recorded for each accepted event. An example of these three signals is given in Fig. 4. For clarity of Fig. 4(a), the thermal emission signal at  $\lambda = 790 \text{ nm}$  (D2) is shifted by 0.2 V. The signals of Fig. 4 are typical signals of particles impacting on the substrate in the center of the optics field of view.

The splat corresponding to the signals in Fig. 4 is shown in Fig. 5 and is typical of those analyzed in this work. These splats have a circular central part of about 70  $\mu\text{m}$  diameter with some spots of material scattered around the core. Another type of splat geometry can also be found. Figure 6 illustrates an example of this splat geometry, in which there is an annulus of material around the circular central part. Although they are not specifically discussed in this work, the signals corresponding to these splats are qualitatively similar to those of Fig. 4.

The in-flight particle parameters are obtained from the analysis of the first two peaks in the thermal emission signals (Fig. 4a). For the events analyzed in this work, the average particle velocity and temperature are 85 m/s and 2790 °C, respectively. The time evolution of the particle surface temperature and equivalent diameter during impact can be computed from the signals collected by the third slit (after 20  $\mu\text{s}$  in Fig. 4a and b). The results corresponding to this computation are given in Fig. 7. During the first 2  $\mu\text{s}$  following the impact at 20  $\mu\text{s}$ , the thermal emission signals increase and, simultaneously, the 690 nm signal decreases.

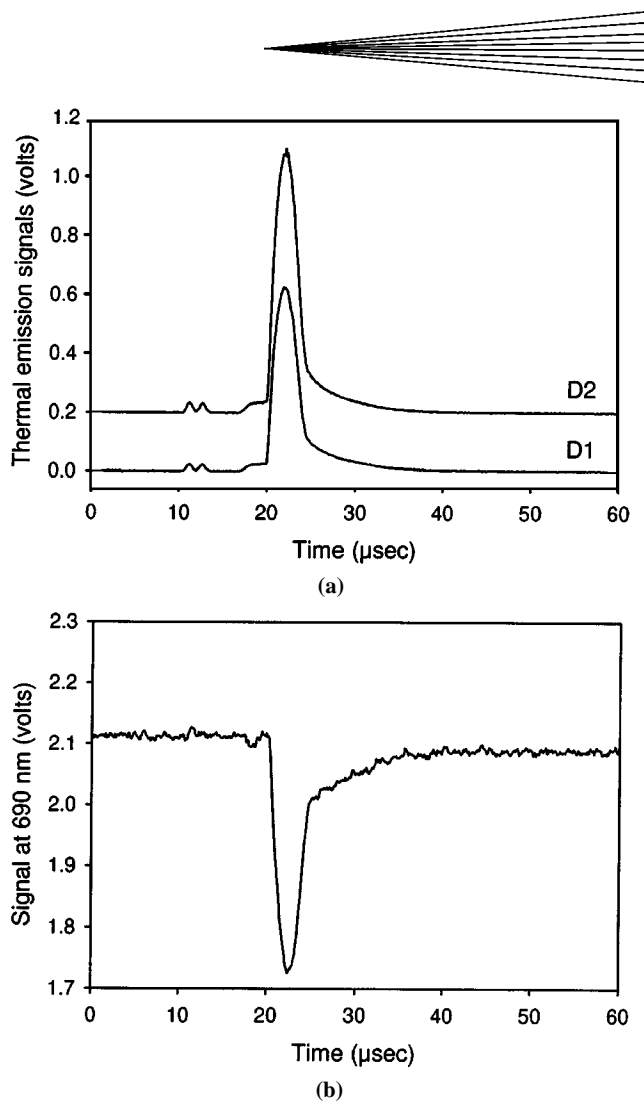


**Fig. 4** Example of collected signals: (a) thermal emission signals and (b) 690 nm signal. In absence of radiation on photodetectors, the three signals are null, except for the signal D2, which is shifted by 0.2 V for clarity

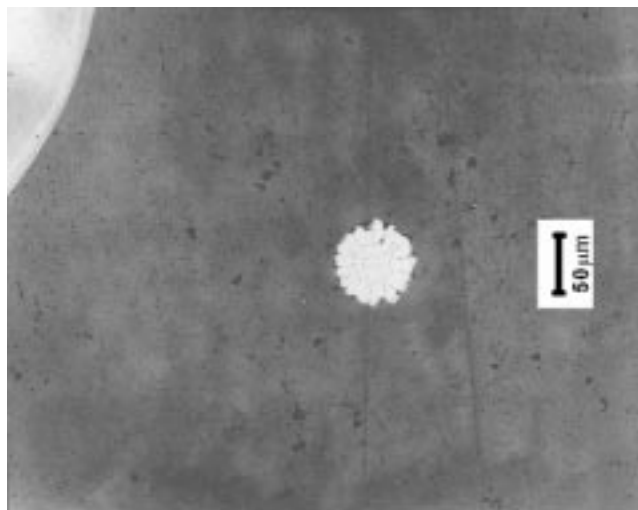


**Fig. 5** Example of a typical molybdenum splat (glass substrate) without annulus of material around the core

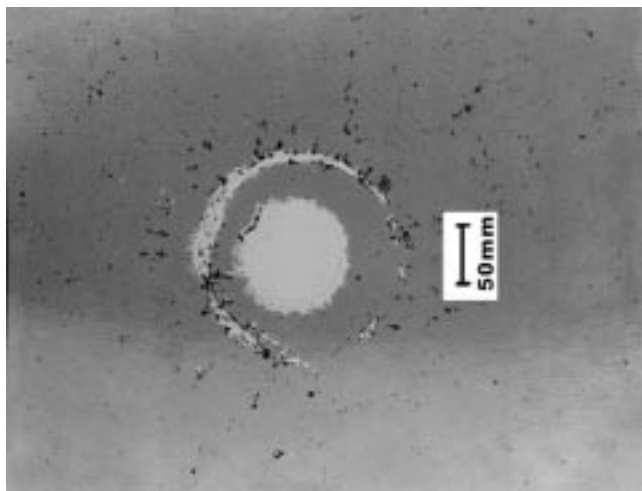


**Fig. 6** Example of a typical molybdenum splat (glass substrate) with an annulus of material around the core

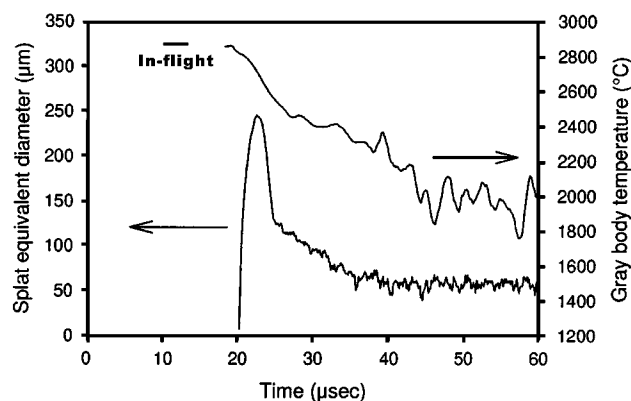


**Fig. 7** Time evolution of equivalent diameter and surface temperature of a molybdenum particle during impact on a smooth glass substrate at room temperature

This corresponds to the spreading of the particle at impact from its initial size to the maximum equivalent diameter of about 250  $\mu\text{m}$  (Fig. 7). The flattening time is measured from the time evolution of the splat equivalent diameter. Its value ranges from 1.5 to 2.5  $\mu\text{s}$  for all analyzed signals and is about 2  $\mu\text{s}$  in the case of Fig. 7. This latter value is similar to the one determined from the thermal emission signals and obtained by measuring the time between the beginning of the impact and the maximum of the thermal radiation signal (Fig. 4a). The agreement between these values shows that the temperature drop occurring during flattening does not have a significant influence on the time the thermal signal is maximum. Indeed, in Fig. 7, the temperature decrease is rather small, from 2820  $^{\circ}\text{C}$  to 2700  $^{\circ}\text{C}$  between the impact and the time the splat size is maximum. More details on the influence of a rapid cooling on flattening measurement from thermal emission signals can be found in Ref 12.

A value of the flattening degree can be obtained from Fig. 4 and 7. The flattening degree is, by definition, the ratio of the final

splat equivalent diameter to the diameter of the (spherical) particle before impact. From the thermal emission signal, a value of the initial flattening degree can be estimated from the ratio of the maximum signal intensity by the two-peak signal intensity (in-flight particle). In the case of Fig. 4(a), the flattening degree is about 7.4. The flattening degree cannot be rigorously estimated from the 690 nm signal, as no reliable information on the particle size before impact can be measured from this signal. However, the maximum splat size measured from laser attenuation is about 250  $\mu\text{m}$  (Fig. 7), and the particles are sieved between 32 and 45  $\mu\text{m}$ , which gives an average flattening degree of  $6.7 \pm 1.1$ . Furthermore, by taking into account a correction for the thermal emission component, the flattening degree measured from the 690 nm signal is  $7.7 \pm 1.3$ , which is in agreement with the 7.4 value measured from pyrometer signals. Consequently, in the situation of the present work, the parameters characterizing the initial flattening can be estimated either from the thermal emission signal or from the signal at 690 nm.

The 690 nm signal decreases during the first 2  $\mu\text{s}$  after impact and is followed by a signal increase between 22 and 40  $\mu\text{s}$  (Fig. 4b). The behavior of the 690 nm signal can be divided according to two time windows. Between 22 and 25  $\mu\text{s}$ , the decrease is rapid with a rate similar to the increase rate between 20 and 22  $\mu\text{s}$ . After about 25  $\mu\text{s}$ , the 690 nm signal continues decreasing but at a rate significantly lower and tending to be null at 40  $\mu\text{s}$ . In other words, after having reached a diameter of 250  $\mu\text{m}$ , the equivalent splat diameter decreases rapidly, down to about 130  $\mu\text{m}$ , and then more slowly to reach about 60  $\mu\text{m}$  at 20  $\mu\text{s}$  after the impact (Fig. 7). Such an evolution of the particle diameter can explain the rapid decrease of the thermal emission signals during the 3  $\mu\text{s}$  after they have reached their maximum value. Indeed, during these 3  $\mu\text{s}$ , the thermal emission signals decrease by a factor of 5, which would correspond to a temperature decrease of about 600 to 750  $^{\circ}\text{C}$  (depending on the considered wavelength) for a given particle surface area. This decrease is not consistent with the temperature decrease (170  $^{\circ}\text{C}$ ) obtained by two-color pyrometry, as already discussed in Ref 13. However, the temperature decrease is consistent with the thermal emission signal behavior if we consider that the particle surface area decreases by a factor 4 during the same period. This decrease of the splat diameter shows also that it can be dangerous to characterize the cooling phenomenon by the time it takes for the monochromatic thermal emission signal to decrease by a given factor.

Before going further in the discussion on the phenomena involved during the first 20  $\mu\text{s}$  after particle impact, it is necessary to validate some of the assumptions leading to the particle diameter measurement during impact. This measurement by laser attenuation is based on two assumptions: first, during the measurement, the flattening material stays inside the square optical field of view of the 510  $\mu\text{m}$  side; and, second, the particle is opaque to the radiation at 690 nm during the entire flattening process. The first assumption was discussed in Ref 13. It was concluded that the decrease of the thermal emission signals during the first microseconds following the maximum of thermal emission signal cannot be related to an exit of material from the optics field of view. This conclusion is still considered valid in this work, where similar spraying conditions are used. In Ref 13, it was mentioned that it is possible that a fraction of the flattening material moves out of the pyrometer field of view, but not in

the first microseconds following the maximum of the thermal emission signal. This is also possible in this case, but certainly not in the 2 to 3  $\mu\text{s}$  after the splat reaches its maximum extent.

The question of an eventual transparency of the molybdenum film has *a priori* to be asked for validation of the diameter measurement. An order of magnitude of the molybdenum film thickness can be estimated by assuming that the spherical in-flight particle becomes a cylinder after impact. With this assumption, for a maximum splat diameter of about 250  $\mu\text{m}$  (Fig. 7) and a 40  $\mu\text{m}$  particle, the average splat thickness is about 0.5  $\mu\text{m}$ . This thickness is of the same order of magnitude as the one measured on molybdenum splats in a previous study.<sup>[13]</sup> Although this thickness is very thin, it is more than one order of magnitude thicker than the molybdenum skin depth at high temperature.<sup>[23]</sup> Then, a 0.5  $\mu\text{m}$  film of metallic molybdenum is opaque, and the measurement of the laser radiation attenuation by this splat can very well be related to its surface area. The problem is more complex when considering that some molybdenum oxidation may occur, because metallic oxides are generally transparent in the visible range. Indeed, it is possible that some molybdenum oxide is formed during the time of flight of the particle and/or during its flattening on the substrate. Data on oxidation rates of molybdenum metal, especially molten, and on the vaporization rate of molybdenum oxides are difficult to find. Consequently, the possibility that there is some oxidation and that the film is partially transparent cannot *a priori* be rejected according to data available on molybdenum. However, some experimental information on molybdenum splats can be extracted from a study of Fukomoto *et al.*<sup>[15]</sup> In this work, there are results on metallic splats deposited on a substrate at high temperature. In the pictures given by Fukomoto, there is no evidence of oxidation and the splats are metallic and thick enough to be opaque in the visible range. These splats are regular (no splashing) with an equivalent diameter of 250 to 300  $\mu\text{m}$ , similar to the one obtained in the present work, where there is some splashing. For splats of equivalent diameter discussed in the present paper, there is then no reason to have more oxidation and vaporization of the molybdenum oxide than in Fukomoto's study. Consequently, from these experimental observations, it is reasonable to think that, if there is some molybdenum oxidation in the present case, it has no significant influence on the opacity of the molybdenum splat.

From the preceding remarks validating the particle diameter measurement, it results that the diameter of the impacting particle decreases by a factor about 2 in the first microseconds after having reached its maximum. During the rapid decrease of the particle diameter, its temperature given by two-color pyrometry decreases by about 170  $^{\circ}\text{C}$  (Fig. 7). In the second time window, from about 25 to 40  $\mu\text{s}$ , the particle diameter decreases from 130 to 60  $\mu\text{m}$  while its temperature decreases from 2550 to 2200  $^{\circ}\text{C}$ . In this second phase, it is possible that a part of the material moves out of the optical field of view, as previously discussed.<sup>[13]</sup> However, if there is some, the fraction of the particle, which is outside the observed zone, is small. For all observed events, the final splat size is found to be within  $\pm 15\%$  of the splat equivalent diameter measured by attenuation. This 15% inaccuracy is consistent with the attenuation measurement accuracy. Indeed, when the sprayed material is completely solidified, the measurement accuracy is lower than at the maximum of flattening, as the final diameter and, then, the attenuation are smaller.

From the results presented above, an explanation can be pro-



posed for the behavior of the particle during the first microseconds after impact. Laser attenuation, thermal emission signals, and microscopic observation of the external contour of the analyzed splats show that the diameter of the particle has reached 250 to 300  $\mu\text{m}$  (equivalent diameter) during the flattening process. This flattening degree is comparable with the values given by Madejski's model.<sup>[1,2,13]</sup> In the present work, during the 2 to 3  $\mu\text{s}$  after the particle reaches its maximum extent, the equivalent diameter of the thin film of molten metal decreases by a factor of 2. According to Madejski, because of viscous dissipation, there is not enough energy after flattening for the material to shrink back to its initial shape in such a short period of time. However, as a metal film of 0.5  $\mu\text{m}$  thickness is very unstable, it can break for a lot of reasons and form contiguous segments. In each of the segments, there is enough surface energy for the material to contract the surface of the segment by a factor of 4 during 2 to 3  $\mu\text{s}$ . This segmentation and contraction can be very rapid, as only a small displacement of material is sufficient. For instance, it is the case if the segmentation is of radial type and transforms the circular splat into a starlike splat. In this explanation, the rapid decrease of the splat surface corresponds to the decrease of the laser attenuation in the 2 to 3  $\mu\text{s}$  following the maximum of attenuation. After these 2 to 3  $\mu\text{s}$ , the splat surface continues decreasing according to the attenuation measurement. This decrease can be explained by the film segmentation, which continues, and also by the fact that some material may exit from the observed zone.

Such an explanation, which has to be validated, allows us to explain the behavior of the optical signals in the first microseconds after the particle impact. The wettability of the substrate by the particle is certainly one of the parameters that controls the segmentation, and then the contraction of the metal film. Indeed, if the metal film does not wet the substrate surface well, its tendency to segment and contract is important in order to minimize the splat surface energy. The substrate temperature is obviously another key parameter, as it controls the molybdenum splat shape.<sup>[15]</sup> It affects both the wettability of the substrate by the molybdenum film and the moment at which nucleation occurs in the splat.

## 4. Conclusions

A new optical technique is described for simultaneous measurement of the thermal emission and surface area of plasma-sprayed particles during impact on a substrate. With this technique, the surface area of a particle during flattening is measured by laser attenuation. Results are presented for molybdenum particles impacting on a smooth glass substrate at room temperature. The splats collected on the substrate present an irregular shape with a central part and splashing of molybdenum around this central part. Measurements of the particle surface area during impact are well correlated with the dimensions of the splats sticking on the substrate and with the flattening degree measured from thermal emission signals. Results show that the particle initially flattens in about 2  $\mu\text{s}$  after impact to reach a 250 to 300  $\mu\text{m}$  equivalent diameter. At that moment, the thickness of the liquid metal film is less than 1  $\mu\text{m}$ . Once the particle has reached its maximum size, its surface area decreases by a factor 4 in 2 to 3  $\mu\text{s}$ . The decrease of the particle surface after the ini-

tial flattening indicates that it can be dangerous to estimate the particle cooling rate from the decrease time of the thermal emission signal. In the proposed explanation, the decrease of the particle surface area corresponds to a segmentation of the thin metal film in different parts, followed by a contraction of the surface of each segment.

In future works, the measurement of the particle surface area during impact on glass substrates at various temperatures will permit evaluation of the validity of the assumptions presented in this work. In particular, the influence of the substrate wettability and of the liquid metal nucleation will be investigated in order to explain the role of the substrate temperature in the splat shape.

### Acknowledgments

The authors thank Mr. Mario Lamontagne for his help with the plasma torch operation and the design of the experimental setup.

This work is based on a presentation made at the 1997 *United Thermal Spray Conference*, Indianapolis, IN, Sept. 1997.

### References

1. J. Madejski: *Int. J. Heat Mass Transfer*, 1976, vol. 19, pp. 1009-13.
2. J. Madejski: *Int. J. Heat Mass Transfer*, 1983, vol. 26 (7), pp. 1095-98.
3. G. Trapaga, E. F. Matthys, J. J. Valencia, and J. Szekely: *Metall. Trans. B*, 1992, vol. 23B, pp. 701-18.
4. T. Watanabe, I. Kuribayashi, T. Honda, and A. Kanzawa: *Chem. Eng. Sci.*, 1992, vol. 47 (12), pp. 3059-65.
5. M. Bertagnolli, M. Marchese, and G. Jacucci: *J. Thermal Spray Technol.*, 1995, vol. 4 (1), pp. 41-49.
6. H. Liu, E. J. Lavernia, and R. H. Rangel: *J. Phys. D: Appl. Phys.*, 1993, vol. 26, pp. 1900-08.
7. A. C. Léger, M. Vardelle, A. Vardelle, P. Fauchais, S. Sampath, C. C. Berndt, and H. Herman: in *Thermal Spray: Practical Solutions for Engineering Problems*, C.C. Berndt, ed., ASM International, Materials Park, OH, 1996, pp. 623-28.
8. M. Pasandideh-Fard and J. Mostaghimi: in *Thermal Spray: Practical Solutions for Engineering Problems*, C. C. Berndt, ed., ASM International, Materials Park, OH, 1996, pp. 637-46.
9. H. Fukunuma: in *Thermal Spray: Practical Solutions for Engineering Problems*, C. C. Berndt, ed., ASM International, Materials Park, OH, 1996, pp. 647-56.
10. A. C. Léger, M. Vardelle, A. Vardelle, B. Dussoubs, and P. Fauchais: in *Thermal Spray Science and Technology*, C. C. Berndt and S. Sampath, eds., ASM International, Materials Park, OH, 1995, pp. 169-74.
11. M. Vardelle, A. Vardelle, A. C. Léger, and P. Fauchais: in *Thermal Spray Industrial Applications*, C. C. Berndt and S. Sampath, eds., ASM International, Materials Park, OH, 1994, pp. 555-62.
12. C. Moreau, P. Cielo, and M. Lamontagne: *J. Thermal Spray Technol.*, 1992, vol. 1 (4), pp. 317-23.
13. C. Moreau, P. Gougeon, and M. Lamontagne: *J. Thermal Spray Technol.*, 1995, vol. 4 (4), pp. 25-33.
14. L. Bianchi, F. Blein, P. Lucchese, M. Vardelle, A. Vardelle, and P. Fauchais: in *Thermal Spray Industrial Applications*, C. C. Berndt and S. Sampath, eds., ASM International, Materials Park, OH, 1994, pp. 569-74.
15. M. Fukumoto, S. Katoh, and I. Okane: in *Thermal Spraying—Current Status and Future Trends*, Akira Ohmori, ed., High Temperature Society of Japan, Osaka, 1995, pp. 353-58.
16. Y. Huang, M. Ohwatari, and M. Fukumoto: in *The Role of Welding Science and Technology in the 21st Century*, M. Ushio, ed., Japan Welding Society, Nagoya, 1996, pp. 731-36.
17. C. Moreau, P. Cielo, M. Lamontagne, S. Dallaire, and M. Vardelle: *Meas. Sci. Technol.*, 1990, vol. 1, pp. 807-14.
18. M. Vardelle, A. Vardelle, P. Fauchais, and C. Moreau: *Meas. Sci. Technol.*, 1994, vol. 5, pp. 205-12.
19. C. Moreau, P. Gougeon, and M. Lamontagne: in *Thermal Spraying—Current Status and Future Trends*, Akira Ohmori, ed., High Temperature Society of Japan, Osaka, 1995, pp. 347-51.
20. P. Gougeon, C. Moreau, V. Lacasse, M. Lamontagne, I. Powell, and A. Bewsher: in *Advanced Processing Techniques—Particulate Materials*, Metal Powder Industries Federation, Princeton, NJ, 1994, vol. 6, pp. 199-210.
21. C. Moreau, P. Gougeon, M. Lamontagne, V. Lacasse, G. Vaudreuil, and P. Cielo: in *Thermal Spray Industrial Applications*, C. C. Berndt and S. Sampath, eds., ASM International, Materials Park, OH, 1994, pp. 431-37.
22. P. Gougeon and C. Moreau: *J. Thermal Spray Technol.*, 1993, vol. 2 (3), pp. 229-33.
23. *Metals Handbook*, 8th ed., vol. 1, *Properties and Selection of Metals*, T. Lyman, ed., ASM, Metals Park, OH, 1961, p. 1216.